Transferable Gaussian Attractive Potentials for Organic/Oxide Interfaces

Jérôme Rey, Sarah Blanck, Paul Clabaut, Sophie Loehlé, Stephan N. Steinmann, Carine Michel

Transferable Gaussian Attractive Potentials for Organic/Oxide Interfaces

Jérôme Rey,[1‡], Sarah Blanck[1,2‡], Paul Clabaut[1], Sophie Loehlé[2], Stephan N. Steinmann[1,], Carine Michel[1,]**

[1] Université de Lyon, École Normale Supérieure de Lyon, CNRS UMR 5182, Laboratoire de Chimie, 46 allée d'Italie, F69364 Lyon, France

[2] Total Marketing & Services, Chemin du Canal – BP 22, 69360, Solaize, France

AUTHOR INFORMATION

Corresponding Authors

*stephan.steinmann@ens-lyon.fr

*carine.michel@ens-lyon.fr

First Authors:

‡ J.R. and S.B. equally contributed to this work.

KEYWORDS. Force Fields; Alumina; Hematite; Adsorption; Organic Surface Films

ABSTRACT

Organic/oxide interfaces play an important role in many areas of chemistry, and in particular for lubrication and corrosion. Molecular dynamics simulations are the method of choice for providing complementary insight to experiments. However, the force fields used to simulate the interaction between molecules and oxide surfaces tend to capture only weak physisorption interactions, discarding the stabilizing Lewis acid/base interactions. We here propose a simple complement to the straightforward molecular mechanics description based on "out-of-the-box"

Lennard-Jones potentials and electrostatic interactions: the addition of an attractive Gaussian potential between reactive sites of the surface and heteroatoms of adsorbed organic molecules, leading to the GLJ potential. The interactions of four oxygenated and four amine molecules with the typical and widespread hematite and γ-alumina surfaces are investigated. The total RMSD for all probed molecules is only 5.7 kcal/mol, and the corresponding percentage 23% over hematite, while on γ-alumina the RMSD is 11.2 kcal/mol, despite using a single parameter for all five chemically inequivalent surface aluminum atoms. Applying GLJ to the simulation of organic films on oxide surfaces demonstrates that mobility of the surfactants is overestimated by the simplistic LJ potential, while GLJ and other qualitatively correct potentials show a strong structuration and slow dynamics of the surface films, as could be expected from the first-principles adsorption energies for model head-groups.

1. INTRODUCTION

Oxide/organic interfaces play a critical role in a wide range of fields, such as heterogeneous catalysis,[1,2] (photo)electrochemistry,[3] biological[4–10] and geological[11,12] interfaces (with the specific case of nanoconfined liquids[13]), corrosion[14] and lubrication.[15,16] In this paper, we will focus on modeling the interaction of organic molecules with typical oxide surfaces of utmost importance: the hematite (0001) surface[17] as well as the γ-alumina (100) and (110) surfaces.[18] Hematite (α-Fe_2O_3) is a common material, observed in minerals[17,19] or formed on iron-containing alloys.[20] Surface properties of hematite are crucial for flotation (useful for resource recovery), wettability, control of water and impurities on steel surfaces,[21–23] or photocatalysis e.g. photoelectrochemical solar water splitting.[24] On the one hand, γ-alumina is a widespread support in heterogeneous catalysis for many processes ranging from petroleum industries to biomass conversion.[25] The understanding of its interface with liquid water and organic molecules is a key point to improve its stability in presence of liquid water.[26–28] On the other hand, γ-alumina is a model for surface oxidized aluminum. Thus, the interaction of γ-alumina with organic molecules is important for metal working, where the understanding of the interactions between the lubricant and the surface is essential to predict the performances of the lubricant.[29]

Ab initio methods are the most versatile and accurate tools when bond breaking and bond formation are involved. This is a typical phenomenon at oxide/organic interfaces when Lewis acid/base chemisorption is involved. Oxide/organic interfaces have been previously investigated using an ab initio molecular dynamics description at the DFT level.[28,30–32]

However, the computational cost of DFT is extremely high which implies typical trajectories of a few tens of picoseconds and thus a limited sampling. This contrasts with the requirements for modeling of interfacial structuration, which typically requires trajectories of about a nanosecond. These time-scales can only be reasonably reached with cheaper simulations methods, i.e., relying on force fields. Most physics-based force fields consider that the interactions at the interface are driven by physisorption and can thus be described by non-bonding terms (i.e. Lennard-Jones (LJ) and electrostatic potentials). Following this philosophy, Lennard-Jones potentials have been fitted to describe the interactions between metals and organic molecules[33] and the Interface Force Field (IFF) has been developed.[34] The CLAY force field,[35] designed for clay minerals and other metallic oxides such as hematite and alumina, has also been used to study interfaces. DFT computations on these oxide surfaces show that Lewis bases (typically O or N functionalized organic molecules) interact strongly (tens of kcal/mol and interatomic distances below 2 Å) with the exposed Al or Fe atoms of alumina and hematite respectively (Lewis acid sites).[29,36–40] Depending on the awareness of this strong binding by the researchers, this strong bonding is ignored and the widely known combination rules for heterogeneous LJ parameters are used without further validation.[41–47] Alternatively, force fields are system-specifically adapted by refitting various LJ-pair interactions or replacing certain terms by Morse or Buckingham potentials.[48–52] This leads to a tedious system setup, which has to be adapted for each molecule/surface pair studied due to a lack of transferability.

Here, we explore a third route: the use of "simple" (but inaccurate) LJ parameters, augmented by an additional non-bonded force field term that is tailored to the near-chemisorption strength of the interactions in question. The near-chemisorption can be dealt with in various ways, see, for instance the literature for metal-water interaction.[53–55] More generally, ReaxFF[56] can describe reactive events at the interface, although at the expense of a challenging, system dependent, parametrization.[57–59] Moving away from the physics-based force field paradigm, machine learning force fields in the form of artificial neural networks or kernel-ridge regression are in rapid expansion, promising high accuracy due to their highly flexible mathematical form.[60–64] This type of force fields have been recently used to investigate the solid/liquid copper/water[65] and zinc oxide/water[66] interfaces, or to identify the active sites on dealloyed gold surfaces.[67] While these methods appear very promising, the training of such a potential and more importantly its transferability is still challenging and requires a tremendous amount of training data.[68]

The strategy developed here is a simple and transferable improvement of usual LJ-based force fields, aiming at significantly better results with a low computational and parametrization cost.

It is inspired by our previous work on metal/water interface where we proposed the efficient GAL force fields that improve both the strength of adsorption and the angular orientation.[55,69] To minimize the computational burden and its implementation, we herein focus on the improvement of the adsorption strength and its corrugation over the surface. This is achieved by supplementing the existing CLAYFF Lennard-Jones force field (LJ) with an anisotropic attractive Gaussian potential, resulting in a Gaussian-Lennard-Jones force field (GLJ). The anisotropic attractive Gaussian potential, at heart of the GAL force fields, is here centered on Lewis-acid sites (Fe or Al for alumina and hematite respectively) of the surface and acts on O and N atoms of adsorbates. The fitting set and procedure can be found in Section 2, while the GLJ performance and transferability is assessed in section 3, where the influence of the force field on the organic film structuration is also briefly discussed.

2. METHODS

DFT calculations

DFT calculations were performed within the CP2K 5.1 framework,[70] using the PBE generalized gradient approximation functional[71] and the Grimme D3 dispersion correction including C9 terms.[72,73] GTH pseudo potentials[74–77] described the core electrons. A mixed Gaussian and plane waves (GPW)[78,79] method was adopted. The valence electron density was developed on a double-zeta DZVP-MOLOPT basis set, while the auxiliary plane wave basis set had a cutoff energy of 400 Ry. During the self-consistent field process (SCF), the energies were converged to 10^{-6} Ha. As hematite is an antiferromagnetic oxide,[36,80] we used the spin-polarized formalism to describe the anti-ferromagnetic electronic structure and the applied DFT+U method with (U-J) set to 5 eV to take into account the strong electronic correlation of the iron 3d electrons.[36]

The bulk structures of hematite and γ-alumina were optimized to forces below 4.5×10^{-4} Ha/bohr. The hematite bulk was described by an extended supercell ($p(3 \times 3 \times 1)$) to be able to restrict the Brillouin zone sampling to the Γ-point for compatibility with the orbital transformation algorithm to converge efficiently the electronic structure of hematite. The γ-Al_2O_3 bulk structure is taken from Digne's bulk model.[18,81] Its geometry was optimized using a $p(1 \times 1 \times 1)$ unit cell also together with a $(3 \times 2 \times 2)$ Monkhorst-Pack[82] k-point grid. In both cases, this set up was found to be the best compromise to limit the error on the cell vectors. On hematite, where experimental data are available,[83] we found an error below 0.5% on the optimized cell vectors.

Surface slab models and molecule adsorption at the DFT level

The surfaces were cleaved from the optimized bulk using a slab of at least 10 Å thickness and a vacuum of at least 30 Å, the coordinates and setup are available in the SI. The central symmetry is preserved, ensuring that the total dipole moment is zero. The slabs were frozen in their bulk geometry during all computations. Keeping the slab frozen upon adsorption has a small impact on the adsorption energies (below 2%). Geometry optimization of molecules on the frozen surfaces were conducted in order to determine the optimal adsorption coordinates for the anchoring atom of each system. These calculations were converged to forces below 4.5×10^{-4} Ha/bohr. Due to the large size of the slabs, Brillouin zone sampling was restricted to the Γ-point.

The (0001) surface of α-Fe_2O_3 is widely used both as a catalyst[17,84] and as a model for steel surfaces.[43,85] It is described here using a p(3 × 3) cell. The primitive cell is represented in Figure 1.a showing that only one type of iron atom is exposed at the surface.

γ-Al_2O_3 is known to expose not only its most stable surface, namely the (100), but also the (110), thus exposing a variety of Al sites.[18,81] The corresponding slabs were prepared by cleavage of the bulk, yielding a p(4 × 3) unit cell for the (100) surface and a p(2 × 2) unit cell for the (110) surface. On the (100) surface (Figure 1.b), all three non-equivalent aluminum atoms are truncated octahedral aluminums coordinated to five oxygen atoms. They are labelled Al_{Va}, Al_{Vb} and A_{Vc}. The fourth exposed Al is equivalent to Al_{Vb} and is labelled $Al_{Vb'}$. The (110) surface (Figure 1.c), features one truncated tetrahedral aluminum atom coordinated to three oxygen atoms, labelled Al_{III}, which is the most reactive one and two non-equivalent truncated octahedral aluminum atoms, Al_{IVa} and Al_{IVb}, coordinated to four oxygen atoms.

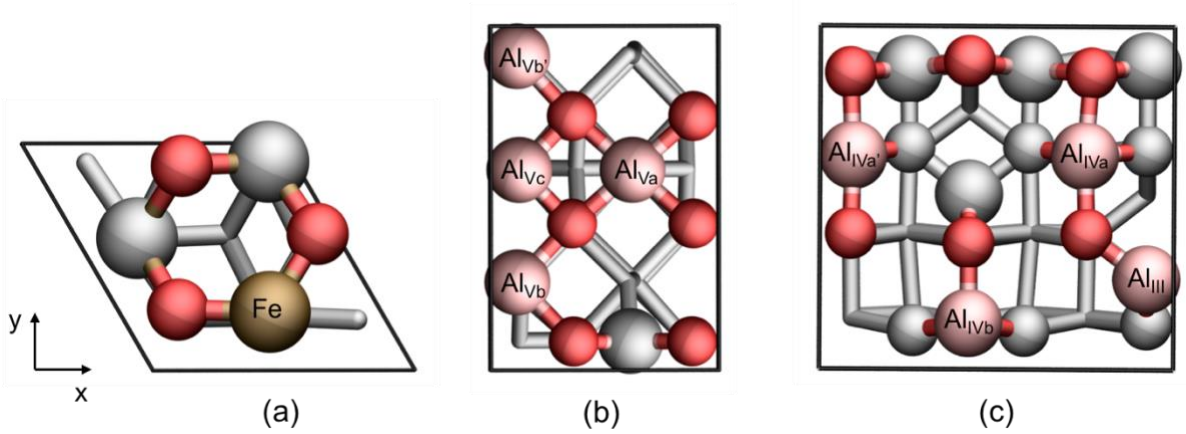

Figure 1. Top view of the p(1x1) unit cell of (a) the (0001) Fe_2O_3 surface, (b) the (100) γ-Al_2O_3 surface and (c) the (110) γ-Al_2O_3 surface. Only exposed atoms are colored (Fe in brown, Al in pink and O in red). Only the first two atomic layers are shown with balls. Equivalent sites are distinguished by a prime.

Molecular Mechanics

Molecular mechanics calculations were also performed with a modified version of CP2K 5.1.[70] The smooth particle-mesh Ewald summation[86] was applied to evaluate the long-range Coulombic interactions. The width parameter was set to 0.36 $Å^{-1}$ and a grid with about 1 point per Å of the corresponding unit-cell length was used.

The Lennard-Jones parameters and the charges of hematite and alumina surfaces were taken from the CLAYFF force field[35] (see Table S1). The GAFF force field[87] was adopted for organic molecules with Gasteiger charges[88] assigned by Open Babel (Table S2)[89] whereas water molecules were described with the flexible TIP3P model.[90,91] As implemented in Ambertools,[92] the Lorentz/Berthelot combining rules were used for interactions involving different atom types. This level of theory is referred to as LJ later on, since the interfacial interactions are only treated through Lennard-Jones potentials and point charges.

In order to improve the description of the interaction of organic molecules with the Lewis acid ssites of the surfaces, anisotropic attractive Gaussian potentials between surface metal atoms *Met* (Al or Fe) and heteroatoms *Het* (N or O) of the organic molecules were added. The general expression of this potential for a given *Met-Het* interaction is as follows:

$$V_{Met-Het}(r_{xy}, r_z) = Ae^{-b_{xy}r_{xy}^2}e^{-b_z r_z^2}, \qquad \textbf{Eq. 1}$$

where *A* is the magnitude of the Gaussian attraction, r_{xy} and r_z are the *Met-Het* distances in the (*x*, *y*) plane and the out of plane (*z*) direction respectively, b_{xy} and b_z are the corresponding width parameters of the Gaussian. The three parameters *A*, b_{xy} and b_z are defined independently for each *Met-Het* pair.

When the LJ level of theory is supplemented by this extra attractive potential, it will be referred to as GLJ and the corresponding total energy writes:

$$E_{GLJ} = E_{LJ} + E_{Gaussian} \qquad \textbf{Eq. 2}$$

where $E_{LJ} = E_{CLAYFF/GAFF/TIP3P}$ is the molecular mechanics energy computed with the relevant force fields and $E_{Gaussian}$ is the sum of the $V_{Met-Het}$ potentials.

Fitting set and procedure

We parametrized the attractive Gaussian for four *Met-Het* interactions: Fe-O, Fe-N, Al-O, Al-N, which correspond to 12 parameters. These parameters were adjusted using a trial-and-error approach that allows to easily emphasize the important features of the profiles. More details can be found in SI (section S.1.2) together with a comparison with an automatized fitting for two interactions. To do so, we chose a specific organic molecule (dimethylether for O and

dimethylamine for N) and a specific site for Al (the Al_{Va} site, which is the most reactive one of the (100) surface[29,81]), while hematite (0001) exposes only one type of iron atoms.

The positions of adsorption sites (x_{opt}, y_{opt}, z_{opt}) were defined as the position of the O or N atom of the adsorbed molecule (dimethylether or dimethylamine) determined at the DFT level. The structures of the fitting set were defined as translation of the molecule with respect to this site using a grid detailed in SI (section S.1.2), corresponding to 159 data points for the alumina surface and 126 for hematite. Internal coordinates of the molecule were replaced by the one of the gas phase geometry at the corresponding level of theory, i.e. DFT or GAFF/TIP3P.

The interaction energy is defined in Eq. 3:

$$\Delta E_{int} = E_{mol@slab} - E_{mol} - E_{slab} \quad \textbf{Eq. 3}$$

where $E_{mol@slab}$, E_{mol} and E_{slab} are the electronic energies of the molecule on the slab, the molecule in vacuum and the slab, respectively.

The parameters *A*, b_{xy} and b_z were adjusted in such a way that the computed GLJ interaction energy ΔE_{int} closely reproduces the DFT one (see Figure S1 in Supporting Information). The values of these parameters are given in Table 1.

Met-Het	*A* (kcal/mol)	b_{xy} (Å^{-2})	b_z (Å^{-2})
Fe-O	–120	0.3	0.4
Fe-N	–231	0.3	0.4
Al-O	–51	0.5	0.2
Al-N	–90	0.6	0.2

Table 1. Fitted parameters for the attractive Gaussian potential for four metal-heteroatoms (Met-Het) interactions

Validation set

We assessed the transferability of the Gaussian parameters obtained from dimethylether and dimethylamine to other molecules (methanol, acetone and water for *Met*-O interaction and ammonia, methylamine and trimethylamine for *Met*-N interaction). Similarly, the transferability of the Al-*Het* parameters fitted on the Al_{Va} site was tested on the other sites of the γ-alumina (100) and (110) surfaces.

Interaction energies were defined and computed consistently with the fitting set on an extensive grid designed to include the attractive potential wells found on each surface but also some more repulsive regions of the potential energy surface. More details about the grid we used are provided in the SI (Section S.1.3).

The performance of the LJ and GLJ were assessed against the DFT interaction energies, but discarding the structures corresponding to an endothermic interaction at the DFT level (ΔE_{int}(DFT) > 0) and the data where the repulsive part of potential energy in LJ was too repulsive (ΔE_{int}(LJ) > 40 kcal/mol) since they typically correspond to structures generated along z axis at z_{opt} – 0.25 Å and only show that the Lennard-Jones potential is too repulsive at short distance, a well-known failure.[93–96]

Application to film structuration

Once parametrized, the Gaussian potentials can be used in order to study the formation of organic films. For that purpose, we ran a 1 ns molecular dynamic simulations at the GLJ level of theory of long chain organic molecules over a completely frozen alumina slab using a 0.5 fs timestep. The temperature was set to 300 K using the Nose-Hoover thermostat. The trajectory was then analyzed removing the first 300 ps corresponding to the equilibration of the system.

The system, composed of 12 N-tetradecyldiethanolamine molecules on a p(4x3) (100) γ-alumina surface, was built in the following way. The organic molecules were placed in a 30 Å high box using PACKMOL[97], at a 2 Å distance perpendicularly to the considered surface. The polar head group of the molecules was forced to be oriented towards the surface by construction. A 30 Å vacuum layer was then added on top of the molecules to avoid interactions between two periodically repeated systems.

3. RESULTS AND DISCUSSION

3.1. Transferability among molecules on hematite surface

In this section, we assess the transferability of the Gaussian parameters obtained for the Fe-O and Fe-N interactions using dimethylether and dimethylamine respectively to other molecules: methanol, water and acetone for oxygenated molecules; methylamine, ammonia and trimethylamine for nitrogenated molecules. Interaction energies for these two sets of four molecules were computed at different heights over the adsorption site, as explained in Section 2 and the results are shown in Figure 2, where the root mean square percentage deviation (RMPD) is given for the entire set, but also individually for each molecule.

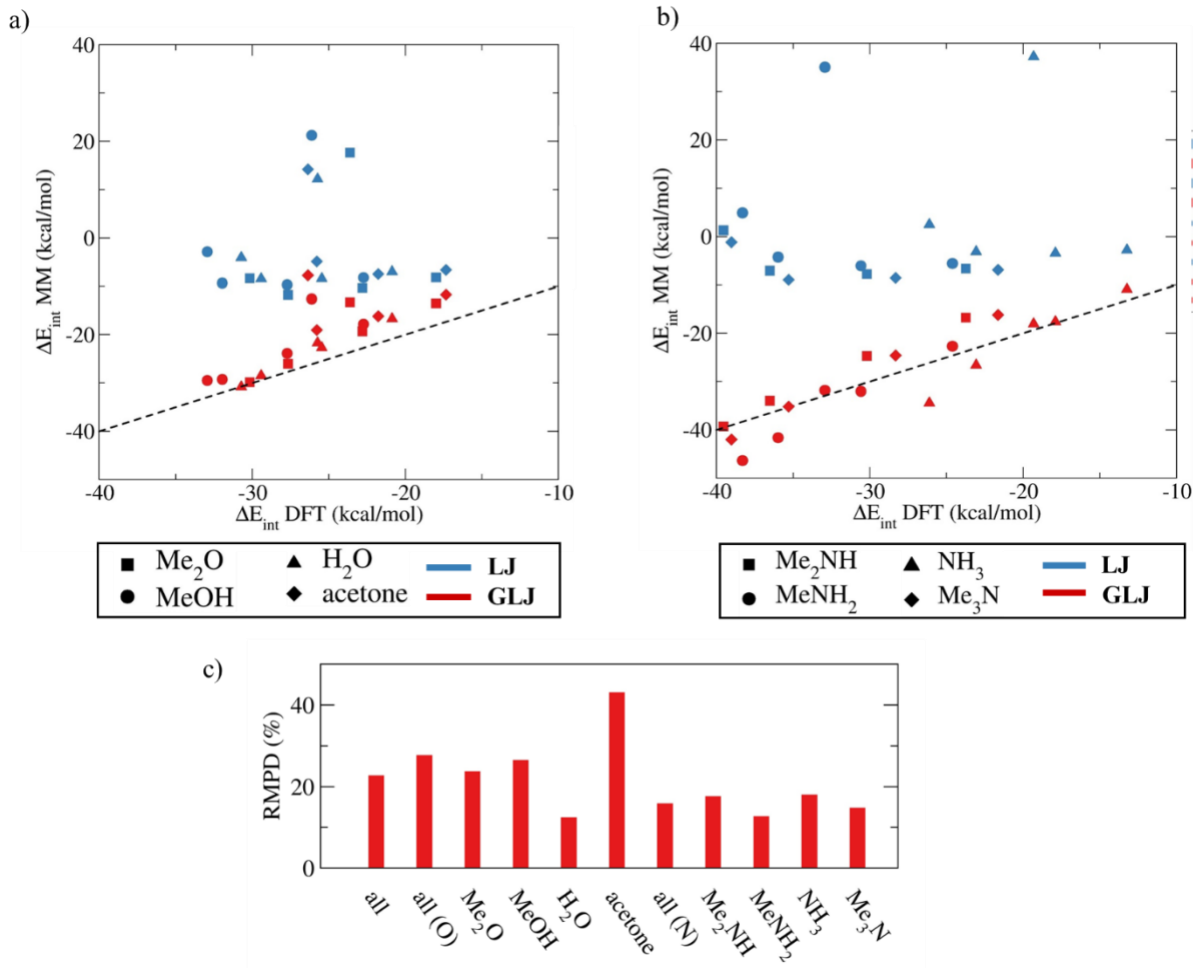

Figure 2. Comparison of the interaction energies of a) oxygenated molecules and b) amines on the hematite (0001) surface computed at the MM level (LJ in blue, GLJ in red) and DFT. c) Corresponding RMPD bar plot for GLJ values.

As expected, the interaction energy is systematically too weak for LJ, and some structures give unrealistic endothermic interaction above 10 kcal/mol. Once supplemented by an attractive Gaussian, GLJ results are much closer to DFT and yield to much stronger, always exothermic, interactions. The root mean square deviation (RMSD) for each molecule is between 2.9 and 6.9 kcal/mol (between 12.6% to 27.5%), demonstrating a good transferability of the Fe-O and Fe-N parameters for the Gaussian attractive potential.

Acetone is the worst case for GLJ (RMSD of 10.7 kcal/mol and RMPD of 43% for GLJ). This does not completely come as a surprise, given that it is the only molecule with a sp^2, rather than a sp^3, oxygen atom. We focused on this challenging case to evaluate if other approaches also found in the literature would constitute a better alternative to GLJ. Using the same fitting set, we considered: (i) a modified LJ for the Fe-O interaction and (ii) a Morse potential (details in SI). We here compare their behavior qualitatively by plotting a z-scan using a fixed orientation

of acetone, i.e. the one found at the fully optimized DFT minimum (Fe-O distance of 2.07 Å, ΔE_{ads} = –32.4 kcal.mol^{-1}). As can be seen in Figure 3, the LJ repulsive part of the potential is too strong. Since the Gaussian attraction cannot compete with the r^{12} repulsive wall, this misrepresentation cannot be corrected with the GLJ potential. Refitting the LJ potential yields to a slightly less repulsive wall (LJmodified, in beige). But this potential seems to underestimate the chemisorption well. In fact, the fixed orientation of acetone is responsible for the rather flat ΔE_{int} at ~ –12 kcal.mol^{-1}. A geometry optimization using this modified LJ locates the minimum at ΔE_{ads} = –135.5 kcal.mol^{-1} with an extremely short Fe-O distance of 1.24 Å (see the optimized structures in Figure S2). This is directly enrooted in the LJ modified parameters with a deep well (84.85 kcal.mol^{-1}) at a very short distance (1.71 Å). This mis-behavior clearly discards the modified LJ. The optimized structure using our GLJ potential or a Morse potential is found at an over-estimated Fe-O distance (2.13 Å and 2.25 Å respectively) with a similar adsorption energy (–26.7 kcal.mol^{-1} and –26.9 kcal.mol^{-1} respectively). The z-scan shows that qualitatively, our GLJ potential is better behaved, with a desorption slope similar to the one found at the DFT level. The mis-behavior of the modified LJ can also lead to strongly structured films on hematite. This is illustrated on the example of n-octadecanamine $C_{18}H_{37}NH_2$ film on hematite in Supporting Information (see Figure S3 and S4).

In summary, the GLJ functional form appears as effective in describing the chemisorption of O and N-containing organic molecules on hematite with a high transferability of the GLJ parameters, fitted on the dimethylether Me_2O or dimethylamine Me_2N, to other molecules with a global RMPD of 23% (see Table S3). This first success of our approach is encouraging, so that we move on to the question of transferability between sites.

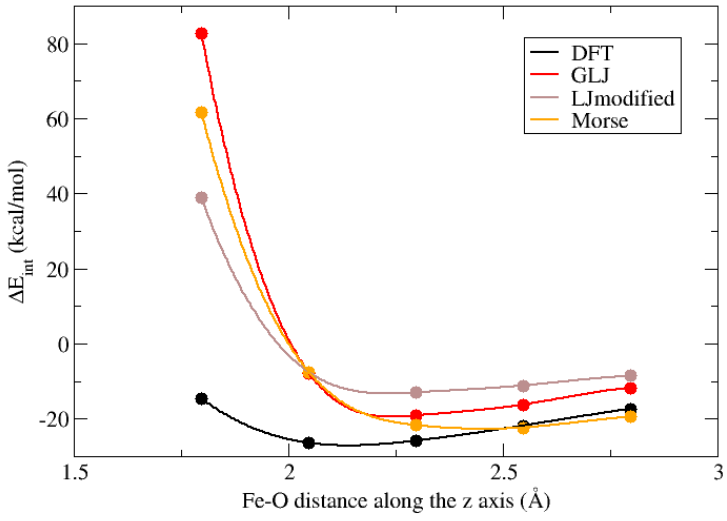

Figure 3. Interaction energies of acetone (gas-phase optimized geometry) with the reactive site of hematite as a function of z. GLJ is the LJ potential derived from the combination rule complemented with an attractive gaussian. LJmodified is a LJ potential that has been refitted on the same data set. Morse is a Morse potential that has been refitted on the same data set. Parameters are provided in Supporting Information.

3.2. Transferability among sites on alumina surface

The transferability of the Gaussian parameters determined for the Al_{Va} to the other five aluminum atoms exposed on γ-alumina (100) and (110) surfaces (see Figure 1) was tested with one probe molecule per *Al-Het* interaction (dimethylether and dimethylamine). The intrinsic acidity ranking of the surface Lewis acid sites is known to be the following: Al_{III} >> Al_{Va} ~ Al_{IVb} > Al_{IVa} > Al_{Vb} >> Al_{Vc}.[81] The GLJ parameters was adjusted on the Al_{Va} site which is of an intermediate acidity and therefore significantly less reactive than Al_{III} and close to Al_{IVb}. The values of interaction energies computed at molecular mechanics levels (LJ and GLJ) are plotted against the DFT interaction energies in Figure 4.

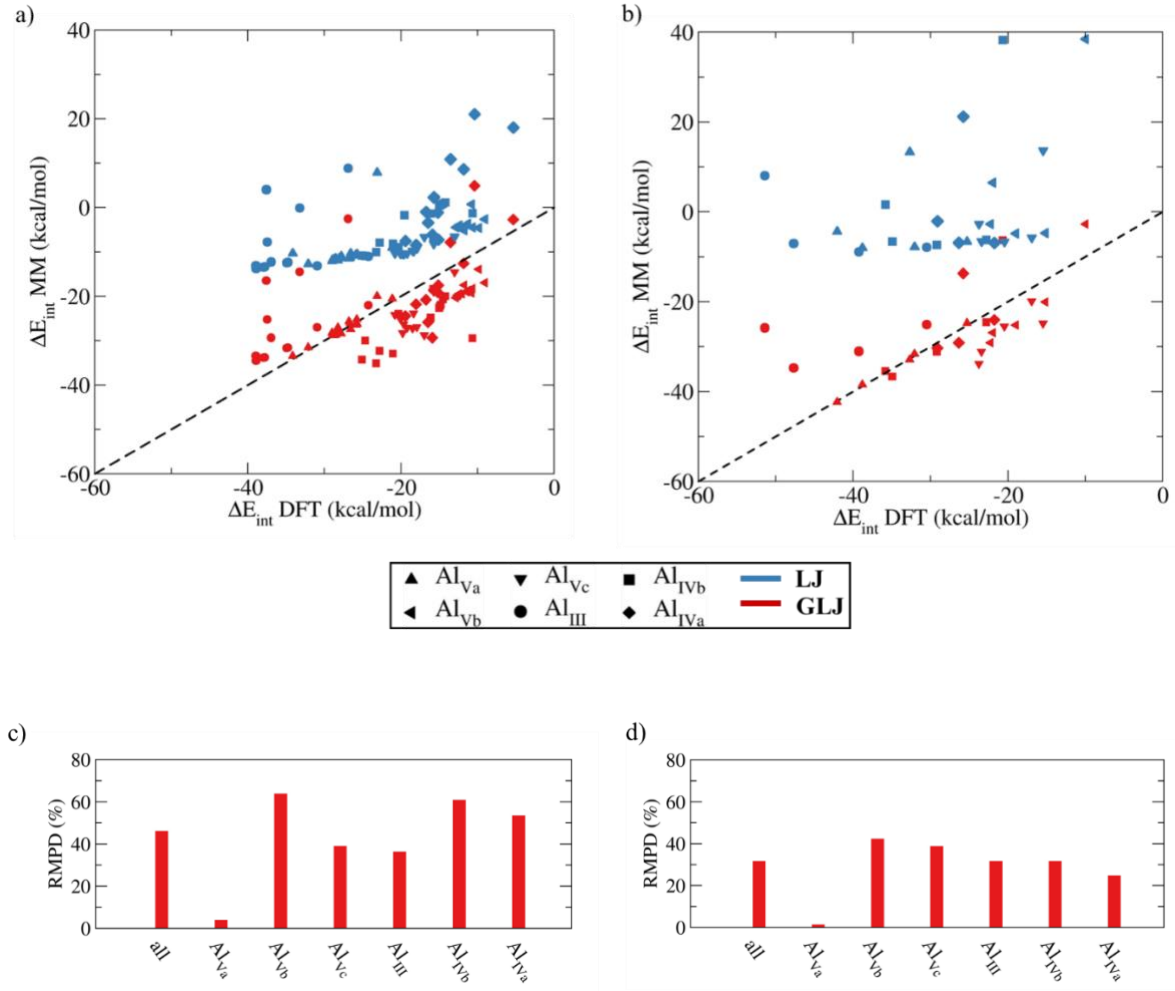

Figure 4. Comparison of interaction energies of (a) dimethyl ether (Me_2O) and (b) dimethyl amine (Me_2NH) on different Al sites computed with molecular mechanics (LJ in blue and GLJ in red) and DFT.

Corresponding RMPD bar plots (percentage) for GLJ values, for dimethyl ether (c) and dimethyl amine (d).

As expected, LJ is largely underbinding for Me_2O and Me_2NH with only small difference between sites, in contrast to DFT. With the Gaussian attractive potential, the interactions computed at the GLJ level are stronger and thus much closer to the DFT values with a root mean square percentage deviation (RMPD) of 46% corresponding to an RMSD of 7.5 kcal/mol.

The attractive Gaussian potential has been fitted on Al_{Va}, (reaching a RMPD of 3.75% for dimethylether and 1.2% for dimethylamine). For the other sites of the (100) surface, which are less reactive, the attractive Gaussian potential is over-binding with respect to DFT, and the RMPD improvement is slightly larger as expected. The Al_{III} site of the (110) surface is the most reactive site studied, significantly more than the Al_{Va} site used to fit the Gaussians parameters. As expected, the GLJ potential remains slightly under-binding near the Al_{III} adsorption site (Figure 5. a) Interaction energies of dimethylether (carbon atom in blue, oxygen of dimethylether in red) with the γ-alumina (110) surface, explored by translation of the adsorbed dimethylether along x axis, starting from the AlIII site.Figure 5). For the less reactive sites of the (110) surface, the RMPD decreases very significantly (see Table S4). In these cases, GLJ becomes over-binding (see Al_{IVb} site on Figure 5.b).

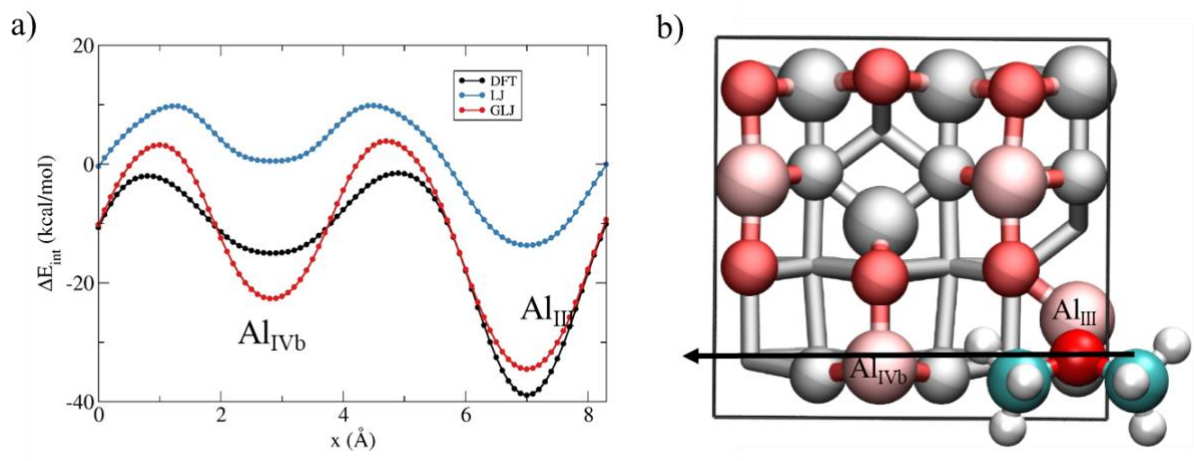

Figure 5. a) Interaction energies of dimethylether (carbon atom in blue, oxygen of dimethylether in red) with the γ-alumina (110) surface, explored by translation of the adsorbed dimethylether along x axis, starting from the Al_{III} site. b) The translation of dimethylether is shown with a black horizontal arrow.

As a conclusion, there is a good overall transferability of the Gaussian parameters between sites, considering that these sites are of different acidities and natures (different coordination of the aluminum atom, tri-, tetra- or penta-coordinated) and that the attractive Gaussian

potential was adjusted on the Al_{Va} site only. Taking into account dimethylether and dimethylamines on all adsorption sites, we reach a RMSD of 7.6 kcal/mol and a RMPD of 43 %. In other words, with a minimal parametrization effort, the adsorption energy profiles are quantitatively improved for all sites of alumina surfaces.

3.3. Transferability among sites and molecules on alumina surface

In this section, we assess the transferability of the Gaussian parameters obtained for Al-O and Al-N using dimethyl ether and dimethylamine to other sites *and* other molecules. Like for hematite, we considered methanol, water and acetone for oxygenated molecules, methylamine, ammonia and trimethylamine for nitrogenated molecules. Interaction energies for these four molecules were computed on the six different adsorption sites of the (110) and (100) γ-alumina surfaces, at different altitudes above these sites, as explained in Section 2. As the transferability of the Gaussian parameters from one site to another has already been investigated in the previous section, we here focus only on the two most reactive sites (Al_{III} and Al_{Va}), while the results for the other sites are reported in Supporting Information (Figures S6 and S7 and Tables S9 to and S11). In Figure 6 the resulting interaction energies obtained at the GLJ level are plotted against the DFT results together with the corresponding RMPD, whereas the LJ results are shown in Figure S5 and RMSD are given in Tables S7 and S8.

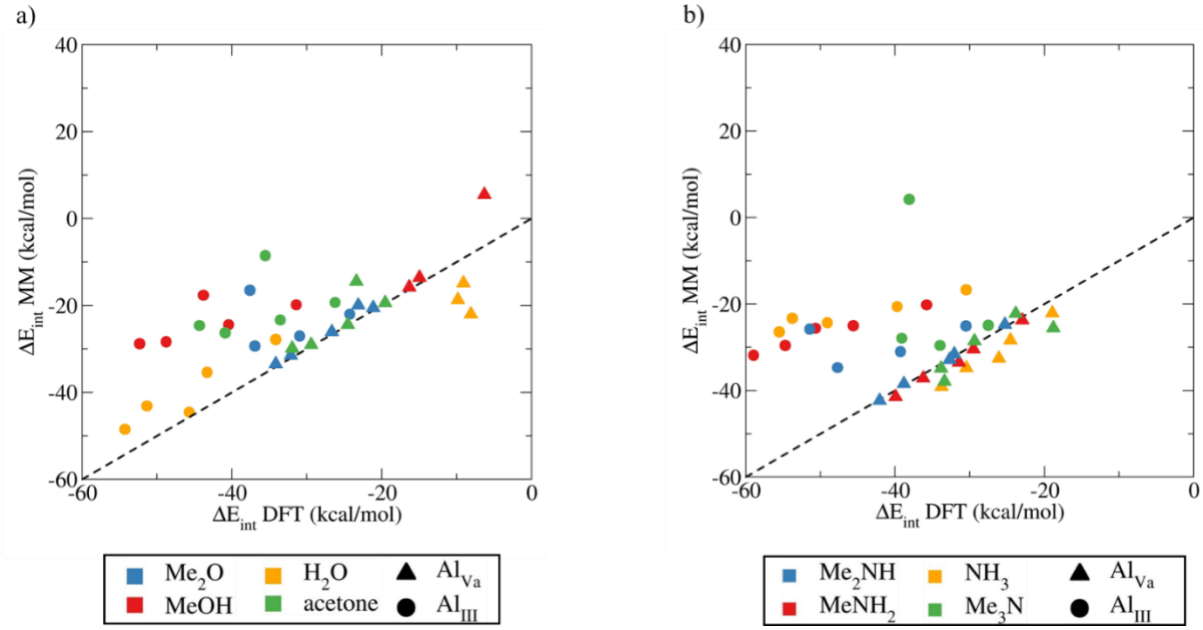

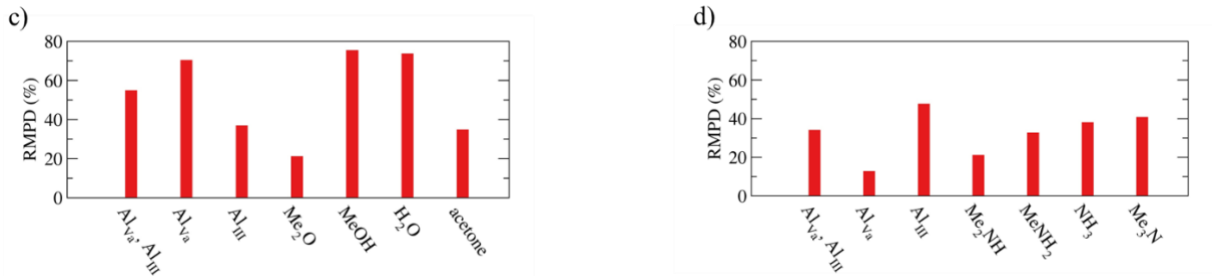

Figure 6. GLJ vs. DFT interaction energies of (a) oxygenated molecules (b) nitrogenated molecules on the most reactive Al site (Al_{III}, squares) and on the site originally used to fit the Gaussian (Al_{Va}, up triangles). Corresponding bar plots for GLJ energies for (c) oxygenated and (d) nitrogenated molecules, in percentage, for all molecules on both sites (labeled all), for all molecules on each site (Al_{Va} and Al_{III}), and for each molecule on both sites.

With GLJ, the interaction of oxygenated (except water) and nitrogenated molecules is consistent with DFT results on Al_{Va}. For example, the RMPD for amines is only 12.7% with a RMSD of 3.1 kcal/mol. This again demonstrates the very good transferability from one molecule to the next of the Gaussian parameters. The interaction of the set of molecules with the more acidic Al_{III} site is even more demanding since it relies on a combined transferability to a more acidic site *and* to another molecule. As expected, given the stronger acidity of Al_{III}, the GLJ interaction of these molecules is still underbinding with a global RMSD of 18.5 kcal/mol and a RMPD of 42.4%.

All in all, the transferability of the GLJ parameters fitted on dimethylether or dimethylamine on the Al_{Va} site to the Al_{III} site and to other molecules is satisfactory. Taking into account all molecules and all adsorption sites (Table S9 to S11), the RMSD decreases significantly by adding the Gaussian potential from 23.7 kcal/mol for the simplistic, combination-rule based LJ potential to 11.2 kcal/mol for GLJ (Table S11).

In other words, without any supplementary parametrization, the attractive Gaussian potential fitted on the interaction of dimethylether or dimethylamine on the Al_{Va} site of the (100) surface can improve the MM description of the interaction of various oxygenated or nitrogenated molecules on (110) and (100) γ-alumina surfaces.

3.4. A case study: Film structuration of long chain ethoxylated amines on γ-alumina (100) surface

Molecular films are important in a variety of application, from tribology to corrosion.[98–100] Typically, fatty amines are used as lubrication additives to beneficiate from their anti-corrosion and friction modification abilities. We demonstrate here the ability of our GLJ forcefield to investigate the structuration of a film on (100) γ-alumina made of a surfactant with a mixed N- and O- polyfunctional head, N-tetradecyldiethanolamine (see Figure 7).

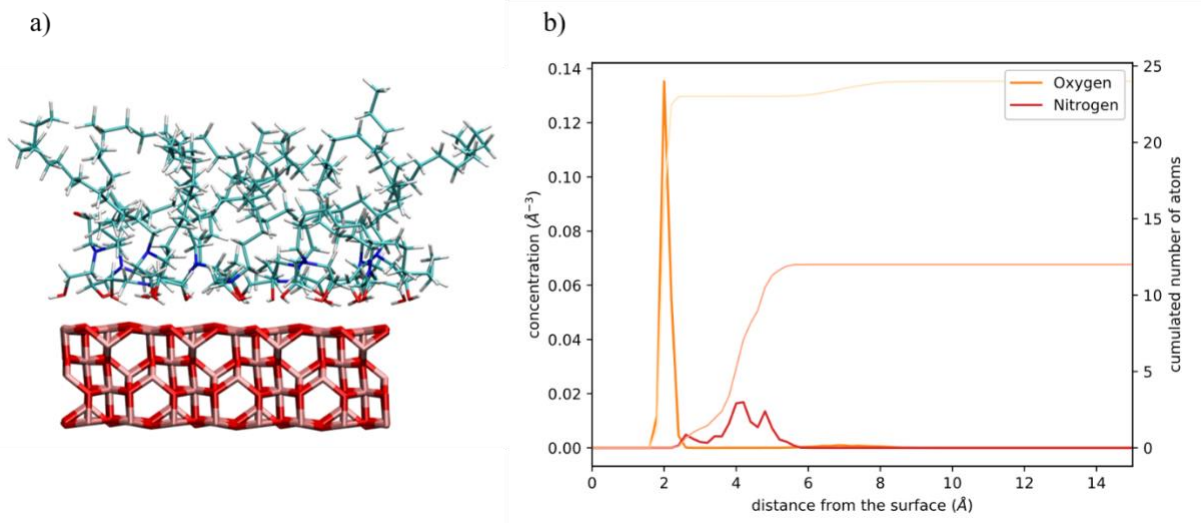

Figure 7. (a) Snapshot of an equilibrated film made of 12 molecules of N-tetradecyldiethanolamine on the (100) surface of γ-alumina (Al in pink, O in red, N in blue, H in white and C in cyan). (b) Concentration of oxygen and nitrogen atoms as a function of the distance to the surface during the GLJ molecular dynamic simulation. The corresponding cumulated number of nitrogen or oxygen atoms is shown with a thin line.

GLJ yields to a much more structured film than LJ according to the density profile (Figure 7b and Figure S8) and the surface concentration in the first 6 Å (see Figure 8 and S9). The significant difference in structuration of the surface film could be responsible for misleading predictions of its properties when using qualitatively inaccurate interfacial force fields.

From the surface concentration profile shown in Figure 7b, it can be seen that N-tetradecyldiethanolamine binds to the surface by its oxygen atoms more likely than by its nitrogen atom. Indeed, oxygen atoms are in average closer (2.0 Å) to the surface than nitrogen atoms (4.2 Å), and the peak for oxygen integrates for 23. The structure of the nitrogen peak is also of interest. While it is rather wide with no noticeable structuration when using LJ (see Figure S8), it splits into several peaks when using GLJ (see Figure 7b), the first small one is positioned at 2.6 Å and integrates for 0.6 atoms. In other words, the inclusion of a differentiated attractive gaussian for the Al-O and Al-N interaction allows the nitrogen atom to interact more closely with the surface.

The structuration within this 6 Å slab in terms of oxygen and nitrogen atom concentration is provided in Figure 8a and b respectively. The 23 oxygen atoms are found in close interaction with the Al sites, the Al_{Vb} site included. Among the 12 nitrogen atoms, three are clearly on top of an Al_{Va} or Al_{Vc} site. All in all, the molecules are more likely adsorbed on Al_{Va} and Al_{Vc} atoms of the surface, which is coherent with the fact that Al_{Va} is the most acidic and therefore the most reactive aluminum atom of the (100) γ-alumina surface.

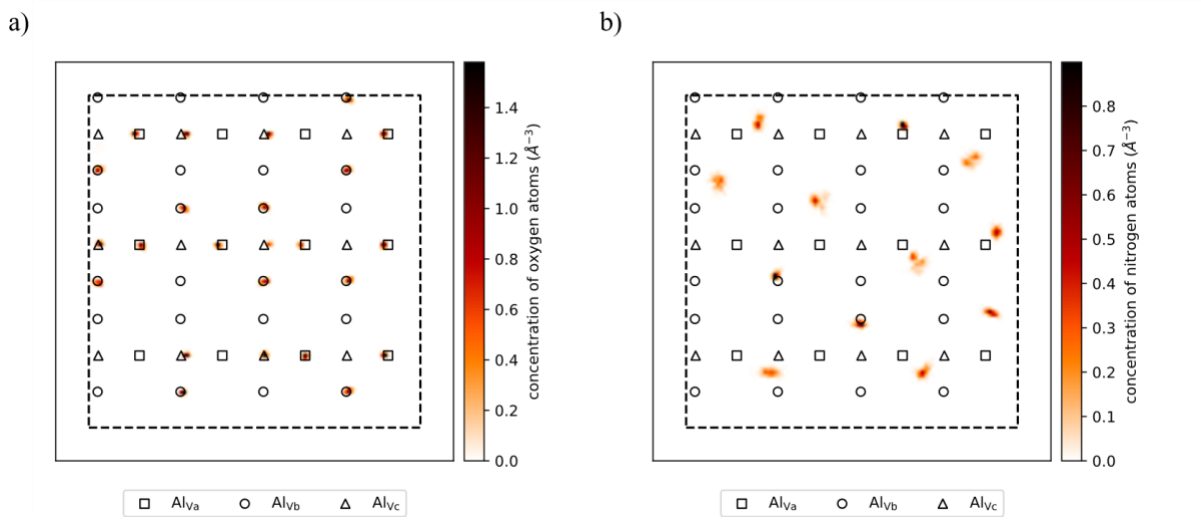

Figure 8. Concentration of (a) oxygen and (b) nitrogen atoms within the first 6 Å above the surface in the xy plane during the GLJ molecular dynamic simulation. Squares, circles and triangles represent the position of the surface aluminum atoms corresponding to Al_{Va}, Al_{Vb} and Al_{Vc} respectively and dotted lines the boundaries of the periodic cell.

4. CONCLUSION

We herein propose a fast and easy to implement improvement of the usual pairwise additive force fields used for surface/molecules interactions. An attractive Gaussian potential is added to the Lennard-Jones potential (GLJ level of theory). The three parameters for a metal-heteroatom interaction were fitted for a typical molecule and a typical surface site and the transferability to other sites and other molecules was extensively tested on two protypical surfaces, hematite and γ-alumina. The transferability between oxygenated and nitrogenated molecules of the same family leads to a significant improvement: the total RMSD for all probed molecules on hematite amounts to 5.7 kcal/mol, and the corresponding percentage to only 23% and to 4.5 kcal/mol and 47.8% on alumina. On γ-alumina, we show that there is a good transferability for the adsorption of dimethylether or dimethylamine fitted on Al_{Va} site to other surface sites (RMSD of 7.6 kcal/mol) and also for our two series of oxygenated and nitrogenated molecules on different sites (RMSD of 11.2 kcal/mol). This improved simple GLJ potential proves useful in the simulation of organic films on oxide surfaces. Indeed, the GLJ potential shows a much stronger structuration and slower dynamics of the surface films compared to the straightforward, but naïve combination-rules based LJ potentials, in agreement with the adsorption energies determined by first principles computations for model head-groups.

SUPPORTING INFORMATION

Supporting Information includes complementary figures and tables, the coordinates of optimal geometries of the chemisorbed molecules and one snapshot of the two interfaces. Coordinates along the molecular dynamics trajectory for the films are provided as zip archive.

ACKNOWLEDGMENTS

This work is part of the project IDEXLYON funded by the French National Research Agency (ANR-16-IDEX-0005), the Commissariat-General for Investment (CGI) and awarded of M€25 (for 4 years) by the French Government within the framework of the Investissements d'Avenir program ("Investment for the Futur"). S. B. gratefully acknowledges Total MS and the ANRT for her PhD fellowship. The authors thank the SYSPROD project and AXELERA Pôle de Compétitivité for financial support (PSMN Data Center). This work was also granted access to the HPC resources of CINES and IDRIS under the allocation 0800609 made by GENCI.

REFERENCES

(1) Sievers, C.; Noda, Y.; Qi, L.; Albuquerque, E. M.; Rioux, R. M.; Scott, S. L. Phenomena Affecting Catalytic Reactions at Solid–Liquid Interfaces. *ACS Catal.* **2016**, *6* (12), 8286–8307. https://doi.org/10.1021/acscatal.6b02532.

(2) Romo, J. E.; Bollar, N. V.; Zimmermann, C. J.; Wettstein, S. G. Conversion of Sugars and Biomass to Furans Using Heterogeneous Catalysts in Biphasic Solvent Systems. *ChemCatChem* **2018**, *10* (21), 4805–4816. https://doi.org/10.1002/cctc.201800926.

(3) Xu, S.; Carter, E. A. Theoretical Insights into Heterogeneous (Photo)Electrochemical CO_2 Reduction. *Chem. Rev.* **2019**, *119* (11), 6631–6669. https://doi.org/10.1021/acs.chemrev.8b00481.

(4) Garley, A.; Hoff, S. E.; Saikia, N.; Jamadagni, S.; Baig, A.; Heinz, H. Adsorption and Substitution of Metal Ions on Hydroxyapatite as a Function of Crystal Facet and Electrolyte PH. *J. Phys. Chem. C* **2019**, *123* (27), 16982–16993. https://doi.org/10.1021/acs.jpcc.9b02808.

(5) Feng, J.; Pandey, R. B.; Berry, R. J.; Farmer, B. L.; Naik, R. R.; Heinz, H. Adsorption Mechanism of Single Amino Acid and Surfactant Molecules to Au {111} Surfaces in Aqueous Solution: Design Rules for Metal-Binding Molecules. *Soft Matter* **2011**, *7* (5), 2113. https://doi.org/10.1039/c0sm01118e.

(6) Wright, L. B.; Rodger, P. M.; Corni, S.; Walsh, T. R. GolP-CHARMM: First-Principles Based Force Fields for the Interaction of Proteins with Au(111) and Au(100). *J. Chem. Theory Comput.* **2013**, *9* (3), 1616–1630. https://doi.org/10.1021/ct301018m.

(7) Brandt, E. G.; Lyubartsev, A. P. Molecular Dynamics Simulations of Adsorption of Amino Acid Side Chain Analogues and a Titanium Binding Peptide on the TiO_2 (100) Surface. *J. Phys. Chem. C* **2015**, *119* (32), 18126–18139. https://doi.org/10.1021/acs.jpcc.5b02670.

(8) Ruan, M.; Seydou, M.; Noel, V.; Piro, B.; Maurel, F.; Barbault, F. Molecular Dynamics Simulation of a RNA Aptasensor. *J. Phys. Chem. B* **2017**, *121* (16), 4071–4080. https://doi.org/10.1021/acs.jpcb.6b12544.

(9) Jiang, W.; Pan, H.; Zhang, Z.; Qiu, S. R.; Kim, J. D.; Xu, X.; Tang, R. Switchable Chiral Selection of Aspartic Acids by Dynamic States of Brushite. *J. Am. Chem. Soc.* **2017**, *139* (25), 8562–8569. https://doi.org/10.1021/jacs.7b03116.

(10) Pham, T. T.; Lemaire, T.; Capiez-Lernout, E.; Lewerenz, M.; To, Q.-D.; Christie, J. K.; Di Tommaso, D.; de Leeuw, N. H.; Naili, S. Properties of Water Confined in Hydroxyapatite Nanopores as Derived from Molecular Dynamics Simulations. *Theor. Chem. Acc.* **2015**, *134* (5), 59. https://doi.org/10.1007/s00214-015-1653-3.

(11) Garcia, N.; Raiteri, P.; Vlieg, E.; Gale, J. Water Structure, Dynamics and Ion Adsorption at the Aqueous {010} Brushite Surface. *Minerals* **2018**, *8* (8), 334. https://doi.org/10.3390/min8080334.

(12) Brugger, J.; Liu, W.; Etschmann, B.; Mei, Y.; Sherman, D. M.; Testemale, D. A Review of the Coordination Chemistry of Hydrothermal Systems, or Do Coordination Changes Make Ore Deposits? *Chem. Geol.* **2016**, *447*, 219–253. https://doi.org/10.1016/j.chemgeo.2016.10.021.

(13) Thompson, W. H. Perspective: Dynamics of Confined Liquids. *J. Chem. Phys.* **2018**, *149* (17), 170901. https://doi.org/10.1063/1.5057759.

(14) Maurice, V.; Marcus, P. Progress in Corrosion Science at Atomic and Nanometric Scales. *Prog. Mater. Sci.* **2018**, *95*, 132–171. https://doi.org/10.1016/j.pmatsci.2018.03.001.

(15) Berro, H.; Fillot, N.; Vergne, P. Molecular Dynamics Simulation of Surface Energy and ZDDP Effects on Friction in Nano-Scale Lubricated Contacts. *Tribol. Int.* **2010**, 12. https://doi.org/10.1016/j.triboint.2010.02.011.

(16) Apóstolo, R. F. G.; Tsagkaropoulou, G.; Camp, P. J. Molecular Adsorption, Self-Assembly, and Friction in Lubricants. *J. Mol. Liq.* **2019**, *277*, 606–612. https://doi.org/10.1016/j.molliq.2018.12.099.
(17) Parkinson, G. S. Iron Oxide Surfaces. *Surf. Sci. Rep.* **2016**, *71* (1), 272–365. https://doi.org/10.1016/j.surfrep.2016.02.001.
(18) Digne, M.; Sautet, P.; Raybaud, P.; Euzen, P.; Toulhoat, H. Use of DFT to Achieve a Rational Understanding of Acid-Basic Properties of γ-Alumina Surfaces. *J. Catal.* **2004**, *226* (1), 54–68. https://doi.org/10.1016/j.jcat.2004.04.020.
(19) Rollmann, G.; Rohrbach, A.; Entel, P.; Hafner, J. First-Principles Calculation of the Structure and Magnetic Phases of Hematite. *Phys. Rev. B* **2004**, *69* (16), 165107. https://doi.org/10.1103/PhysRevB.69.165107.
(20) Chia, C.-L.; Avendaño, C.; Siperstein, F. R.; Filip, S. Liquid Adsorption of Organic Compounds on Hematite α-Fe_2O_3 Using ReaxFF. *Langmuir* **2017**, *33* (42), 11257–11263. https://doi.org/10.1021/acs.langmuir.7b02374.
(21) Shrimali, K.; Jin, J.; Hassas, B. V.; Wang, X.; Miller, J. D. The Surface State of Hematite and Its Wetting Characteristics. *J. Colloid Interface Sci.* **2016**, *477*, 16–24. https://doi.org/10.1016/j.jcis.2016.05.030.
(22) Lane, J. M. D.; Leung, K.; Thompson, A. P.; Cuneo, M. E. Water Desorption from Rapidly-Heated Metal Oxide Surfaces—First Principles, Molecular Dynamics, and the Temkin Isotherm. *J. Phys. Condens. Matter* **2018**, *30* (46), 465002. https://doi.org/10.1088/1361-648X/aae4af.
(23) Foucaud, Y.; Badawi, M.; Filippov, L.; Filippova, I.; Lebègue, S. A Review of Atomistic Simulation Methods for Surface Physical-Chemistry Phenomena Applied to Froth Flotation. *Miner. Eng.* **2019**, *143*, 106020. https://doi.org/10.1016/j.mineng.2019.106020.
(24) Sivula, K.; Le Formal, F.; Grätzel, M. Solar Water Splitting: Progress Using Hematite (α-Fe_2O_3) Photoelectrodes. *ChemSusChem* **2011**, *4* (4), 432–449. https://doi.org/10.1002/cssc.201000416.
(25) Euzen, P.; Raybaud, P.; Krokidis, X.; Toulhoat, H.; Le Loarer, J.-L.; Jolivet, J.-P.; Froidefond, C. Alumina. In *Handbook of Porous Solids*; Schth, F., Sing, K. S. W., Weitkamp, J., Eds.; Wiley-VCH Verlag GmbH: Weinheim, Germany, 2002; pp 1591–1677. https://doi.org/10.1002/9783527618286.ch23b.
(26) Copeland, J. R.; Shi, X.-R.; Sholl, D. S.; Sievers, C. Surface Interactions of C2 and C3 Polyols with γ-Al2O3 and the Role of Coadsorbed Water. *Langmuir* **2013**, *29* (2), 581–593. https://doi.org/10.1021/la304074x.
(27) Réocreux, R.; Girel, É.; Clabaut, P.; Tuel, A.; Besson, M.; Chaumonnot, A.; Cabiac, A.; Sautet, P.; Michel, C. Reactivity of Shape-Controlled Crystals and Metadynamics Simulations Locate the Weak Spots of Alumina in Water. *Nat. Commun.* **2019**, *10* (1), 3139. https://doi.org/10.1038/s41467-019-10981-9.
(28) Ngouana-Wakou, B. F.; Cornette, P.; Corral Valero, M.; Costa, D.; Raybaud, P. An Atomistic Description of the γ-Alumina/Water Interface Revealed by Ab Initio Molecular Dynamics. *J. Phys. Chem. C* **2017**, *121* (19), 10351–10363. https://doi.org/10.1021/acs.jpcc.7b00101.
(29) Blanck, S.; Loehlé, S.; Steinmann, S. N.; Michel, C. Adhesion of Lubricant on Aluminium through Adsorption of Additive Head-Groups on γ-Alumina: A DFT Study. *Tribol. Int.* **2020**, *145*, 106140. https://doi.org/10.1016/j.triboint.2019.106140.
(30) Réocreux, R.; Jiang, T.; Iannuzzi, M.; Michel, C.; Sautet, P. Structuration and Dynamics of Interfacial Liquid Water at Hydrated γ-Alumina Determined by Ab Initio Molecular Simulations: Implications for Nanoparticle Stability. *ACS Appl. Nano Mater.* **2018**, *1* (1), 191–199. https://doi.org/10.1021/acsanm.7b00100.

(31) von Rudorff, G. F.; Jakobsen, R.; Rosso, K. M.; Blumberger, J. Hematite(001)-Liquid Water Interface from Hybrid Density Functional-Based Molecular Dynamics. *J. Phys. Condens. Matter* **2016**, *28* (39), 394001. https://doi.org/10.1088/0953-8984/28/39/394001.
(32) Motta, A.; Gaigeot, M.-P.; Costa, D. AIMD Evidence of Inner Sphere Adsorption of Glycine on a Stepped (101) Boehmite AlOOH Surface. *J. Phys. Chem. C* **2012**, *116* (44), 23418–23427. https://doi.org/10.1021/jp307565p.
(33) Heinz, H.; Vaia, R. A.; Farmer, B. L.; Naik, R. R. Accurate Simulation of Surfaces and Interfaces of Face-Centered Cubic Metals Using 12−6 and 9−6 Lennard-Jones Potentials. *J. Phys. Chem. C* **2008**, *112* (44), 17281–17290. https://doi.org/10.1021/jp801931d.
(34) Heinz, H.; Lin, T. J.; Mishra, R. K.; Emami, F. S. Thermodynamically Consistent Force Fields for the Assembly of Inorganic, Organic, and Biological Nanostructures: The INTERFACE Force Field. *Langmuir* **2012**, *29* (6), 1754–1765. https://doi.org/10.1021/la3038846.
(35) Cygan, R. T.; Liang, J.-J.; Kalinichev, A. G. Molecular Models of Hydroxide, Oxyhydroxide, and Clay Phases and the Development of a General Force Field. *J. Phys. Chem. B* **2004**, *108* (4), 1255–1266. https://doi.org/10.1021/jp0363287.
(36) Dzade, N.; Roldan, A.; de Leeuw, N. A Density Functional Theory Study of the Adsorption of Benzene on Hematite (α-Fe2O3) Surfaces. *Minerals* **2014**, *4* (1), 89–115. https://doi.org/10.3390/min4010089.
(37) Gattinoni, C.; Ewen, J. P.; Dini, D. Adsorption of Surfactants on α-Fe_2O_3 (0001): A Density Functional Theory Study. *J. Phys. Chem. C* **2018**, *122* (36), 20817–20826. https://doi.org/10.1021/acs.jpcc.8b05899.
(38) Arrouvel, C.; Diawara, B.; Costa, D.; Marcus, P. DFT Periodic Study of the Adsorption of Glycine on the Anhydrous and Hydroxylated (0001) Surfaces of α-Alumina. *J. Phys. Chem. C* **2007**, *111* (49), 18164–18173. https://doi.org/10.1021/jp0741408.
(39) Wischert, R.; Laurent, P.; Copéret, C.; Delbecq, F.; Sautet, P. γ-Alumina: The Essential and Unexpected Role of Water for the Structure, Stability, and Reactivity of "Defect" Sites. *J. Am. Chem. Soc.* **2012**, *134* (35), 14430–14449. https://doi.org/10.1021/ja3042383.
(40) Blanck, S.; Martí, C.; Loehlé, S.; Steinmann, S. N.; Michel, C. (Dis)Similarities of Adsorption of Diverse Functional Groups over Alumina and Hematite Depending on the Surface State. *J. Chem. Phys.* **2021**, *154* (8), 084701. https://doi.org/10.1063/5.0038412.
(41) Xie, W. K.; Sun, Y. Z.; Liu, H. T. Atomistic Investigation on the Detachment of Oil Molecules from Defective Alumina Surface. *Appl. Surf. Sci.* **2017**, *426*, 504–513. https://doi.org/10.1016/j.apsusc.2017.07.163.
(42) Doig, M.; Warrens, C. P.; Camp, P. J. Structure and Friction of Stearic Acid and Oleic Acid Films Adsorbed on Iron Oxide Surfaces in Squalane. *Langmuir* **2014**, *30* (1), 186–195. https://doi.org/10.1021/la404024v.
(43) Ewen, J. P.; Gattinoni, C.; Morgan, N.; Spikes, H. A.; Dini, D. Nonequilibrium Molecular Dynamics Simulations of Organic Friction Modifiers Adsorbed on Iron Oxide Surfaces. *Langmuir* **2016**, *32* (18), 4450–4463. https://doi.org/10.1021/acs.langmuir.6b00586.
(44) Olsen, R.; Leirvik, K. N.; Kvamme, B. Adsorption Characteristics of Glycols on Calcite and Hematite. *AIChE J.* **2019**, *65* (11). https://doi.org/10.1002/aic.16728.
(45) Phan, A.; Cole, D. R.; Striolo, A. Preferential Adsorption from Liquid Water–Ethanol Mixtures in Alumina Pores. *Langmuir* **2014**, *30* (27), 8066–8077. https://doi.org/10.1021/la501177t.
(46) Yeh, I.-C.; Lenhart, J. L.; Orlicki, J. A.; Rinderspacher, B. C. Molecular Dynamics Simulation Study of Adsorption of Bioinspired Oligomers on Alumina Surfaces. *J. Phys. Chem. B* **2019**, *123* (32), 7024–7035. https://doi.org/10.1021/acs.jpcb.9b04473.

(47) Xiong, H.; Devegowda, D.; Huang, L. Water Bridges in Clay Nanopores: Mechanisms of Formation and Impact on Hydrocarbon Transport. *Langmuir* **2020**, *36* (3), 723–733. https://doi.org/10.1021/acs.langmuir.9b03244.
(48) Kerisit, S. Water Structure at Hematite–Water Interfaces. *Geochim. Cosmochim. Acta* **2011**, *75* (8), 2043–2061. https://doi.org/10.1016/j.gca.2011.01.026.
(49) Boily, J.-F.; Yeşilbaş, M.; Md. Musleh Uddin, M.; Baiqing, L.; Trushkina, Y.; Salazar-Alvarez, G. Thin Water Films at Multifaceted Hematite Particle Surfaces. *Langmuir* **2015**, *31* (48), 13127–13137. https://doi.org/10.1021/acs.langmuir.5b03167.
(50) Latorre, C. A.; Ewen, J. P.; Gattinoni, C.; Dini, D. Simulating Surfactant–Iron Oxide Interfaces: From Density Functional Theory to Molecular Dynamics. *J. Phys. Chem. B* **2019**, *123* (31), 6870–6881. https://doi.org/10.1021/acs.jpcb.9b02925.
(51) Pominov, A.; Müller-Hillebrand, J.; Träg, J.; Zahn, D. Interaction Models and Molecular Simulation Systems of Steel–Organic Friction Modifier Interfaces. *Tribol. Lett.* **2021**, *69* (1), 14. https://doi.org/10.1007/s11249-020-01384-9.
(52) Valadez Huerta, G.; Raabe, G. Genetic Parameterization of Interfacial Force Fields Based on Classical Bulk Force Fields and Ab Initio Data: Application to the Methanol-ZnO Interfaces. *J. Chem. Inf. Model.* **2020**, *60* (12), 6033–6043. https://doi.org/10.1021/acs.jcim.0c01093.
(53) Siepmann, J. I.; Sprik, M. Influence of Surface Topology and Electrostatic Potential on Water/Electrode Systems. *J. Chem. Phys.* **1995**, *102* (1), 511–524. https://doi.org/10.1063/1.469429.
(54) Spohr, E.; Heinzinger, K. Molecular Dynamics Simulation of a Water/Metal Interface. *Chem. Phys. Lett.* **1986**, *123* (3), 218–221. https://doi.org/10.1016/0009-2614(86)80016-1.
(55) Steinmann, S. N.; Ferreira De Morais, R.; Götz, A. W.; Fleurat-Lessard, P.; Iannuzzi, M.; Sautet, P.; Michel, C. Force Field for Water over Pt(111): Development, Assessment, and Comparison. *J. Chem. Theory Comput.* **2018**, *14* (6), 3238–3251. https://doi.org/10.1021/acs.jctc.7b01177.
(56) van Duin, A. C. T.; Dasgupta, S.; Lorant, F.; Goddard, W. A. ReaxFF: A Reactive Force Field for Hydrocarbons. *J. Phys. Chem. A* **2001**, *105* (41), 9396–9409. https://doi.org/10.1021/jp004368u.
(57) Pitman, M. C.; van Duin, A. C. T. Dynamics of Confined Reactive Water in Smectite Clay–Zeolite Composites. *J. Am. Chem. Soc.* **2012**, *134* (6), 3042–3053. https://doi.org/10.1021/ja208894m.
(58) Ojwang, J. G. O.; van Santen, R. A.; Kramer, G. J.; van Duin, A. C. T.; Goddard, W. A. Parametrization of a Reactive Force Field for Aluminum Hydride. *J. Chem. Phys.* **2009**, *131* (4), 044501. https://doi.org/10.1063/1.3182853.
(59) Shchygol, G.; Yakovlev, A.; Trnka, T.; van Duin, A. C. T.; Verstraelen, T. ReaxFF Parameter Optimization with Monte-Carlo and Evolutionary Algorithms: Guidelines and Insights. *J. Chem. Theory Comput.* **2019**, *15* (12), 6799–6812. https://doi.org/10.1021/acs.jctc.9b00769.
(60) Zeni, C.; Rossi, K.; Glielmo, A.; Baletto, F. On Machine Learning Force Fields for Metallic Nanoparticles. *Adv. Phys. X* **2019**, *4* (1), 1654919. https://doi.org/10.1080/23746149.2019.1654919.
(61) Singraber, A.; Behler, J.; Dellago, C. Library-Based *LAMMPS* Implementation of High-Dimensional Neural Network Potentials. *J. Chem. Theory Comput.* **2019**, *15* (3), 1827–1840. https://doi.org/10.1021/acs.jctc.8b00770.
(62) Dral, P. O. Quantum Chemistry in the Age of Machine Learning. *J. Phys. Chem. Lett.* **2020**, *11* (6), 2336–2347. https://doi.org/10.1021/acs.jpclett.9b03664.

(63) Gkeka, P.; Stoltz, G.; Barati Farimani, A.; Belkacemi, Z.; Ceriotti, M.; Chodera, J. D.; Dinner, A. R.; Ferguson, A. L.; Maillet, J.-B.; Minoux, H.; Peter, C.; Pietrucci, F.; Silveira, A.; Tkatchenko, A.; Trstanova, Z.; Wiewiora, R.; Lelièvre, T. Machine Learning Force Fields and Coarse-Grained Variables in Molecular Dynamics: Application to Materials and Biological Systems. *J. Chem. Theory Comput.* **2020**, *16* (8), 4757–4775. https://doi.org/10.1021/acs.jctc.0c00355.
(64) Bartók, A. P.; De, S.; Poelking, C.; Bernstein, N.; Kermode, J. R.; Csányi, G.; Ceriotti, M. Machine Learning Unifies the Modeling of Materials and Molecules. *Sci. Adv.* **2017**, *3* (12), e1701816. https://doi.org/10.1126/sciadv.1701816.
(65) Natarajan, S. K.; Behler, J. Neural Network Molecular Dynamics Simulations of Solid–Liquid Interfaces: Water at Low-Index Copper Surfaces. *Phys. Chem. Chem. Phys.* **2016**, *18* (41), 28704–28725. https://doi.org/10.1039/C6CP05711J.
(66) Quaranta, V.; Behler, J.; Hellström, M. Structure and Dynamics of the Liquid–Water/Zinc-Oxide Interface from Machine Learning Potential Simulations. *J. Phys. Chem. C* **2019**, *123* (2), 1293–1304. https://doi.org/10.1021/acs.jpcc.8b10781.
(67) Chen, Y.; Huang, Y.; Cheng, T.; Goddard, W. A. Identifying Active Sites for CO_2 Reduction on Dealloyed Gold Surfaces by Combining Machine Learning with Multiscale Simulations. *J. Am. Chem. Soc.* **2019**, *141* (29), 11651–11657. https://doi.org/10.1021/jacs.9b04956.
(68) Noé, F.; Tkatchenko, A.; Müller, K.-R.; Clementi, C. Machine Learning for Molecular Simulation. *Annu. Rev. Phys. Chem.* **2020**, *71* (1), 361–390. https://doi.org/10.1146/annurev-physchem-042018-052331.
(69) Clabaut, P.; Fleurat-Lessard, P.; Michel, C.; Steinmann, S. N. Ten Facets, One Force Field: The GAL19 Force Field for Water–Noble Metal Interfaces. *J. Chem. Theory Comput.* **2020**, *16* (7), 4565–4578. https://doi.org/10.1021/acs.jctc.0c00091.
(70) Hutter, J.; Iannuzzi, M.; Schiffmann, F.; VandeVondele, J. CP2K: Atomistic Simulations of Condensed Matter Systems. *Wiley Interdiscip. Rev. Comput. Mol. Sci.* **2014**, *4* (1), 15–25. https://doi.org/10.1002/wcms.1159.
(71) Perdew, J. P.; Burke, K.; Ernzerhof, M. Generalized Gradient Approximation Made Simple. *Phys. Rev. Lett.* **1996**, *77* (18), 3865–3868. https://doi.org/10.1103/PhysRevLett.77.3865.
(72) Grimme, S.; Antony, J.; Ehrlich, S.; Krieg, H. A Consistent and Accurate Ab Initio Parametrization of Density Functional Dispersion Correction (DFT-D) for the 94 Elements H-Pu. *J Chem Phys* **2010**, *132* (15), 154104. https://doi.org/10.1063/1.3382344.
(73) Grimme, S.; Ehrlich, S.; Goerigk, L. Effect of the Damping Function in Dispersion Corrected Density Functional Theory. *J. Comput. Chem.* **2011**, *32* (7), 1456–1465. https://doi.org/10.1002/jcc.21759.
(74) Hartwigsen, C.; Goedecker, S.; Hutter, J. Relativistic Separable Dual-Space Gaussian Pseudopotentials from H to Rn. *Phys. Rev. B* **1998**, *58* (7), 3641–3662. https://doi.org/10.1103/PhysRevB.58.3641.
(75) Goedecker, S.; Teter, M.; Hutter, J. Separable Dual-Space Gaussian Pseudopotentials. *Phys. Rev. B* **1996**, *54* (3), 1703–1710. https://doi.org/10.1103/PhysRevB.54.1703.
(76) Krack, M. Pseudopotentials for H to Kr Optimized for Gradient-Corrected Exchange-Correlation Functionals. *Theor. Chem. Acc.* **2005**, *114* (1–3), 145–152. https://doi.org/10.1007/s00214-005-0655-y.
(77) VandeVondele, J.; Hutter, J. Gaussian Basis Sets for Accurate Calculations on Molecular Systems in Gas and Condensed Phases. *J. Chem. Phys.* **2007**, *127* (11), 114105. https://doi.org/10.1063/1.2770708.

(78) Lippert, G.; Hutter, J.; Parrinello, M. A Hybrid Gaussian and Plane Wave Density Functional Scheme. *Mol. Phys.* **1997**, *92* (3), 477–487. https://doi.org/10.1080/00268979709482119.
(79) VandeVondele, J.; Krack, M.; Mohamed, F.; Parrinello, M.; Chassaing, T.; Hutter, J. Quickstep: Fast and Accurate Density Functional Calculations Using a Mixed Gaussian and Plane Waves Approach. *Comput. Phys. Commun.* **2005**, *167* (2), 103–128. https://doi.org/10.1016/j.cpc.2004.12.014.
(80) An, J.; Wanaguru, P.; Xia, C.; Tao, M.; Zhang, Q. First-Principles Study of Sulfur Atom Doping and Adsorption on α–Fe2O3 (0001) Film. *Phys. Lett. A* **2016**, *380* (38), 3149–3154. https://doi.org/10.1016/j.physleta.2016.07.042.
(81) Digne, M.; Sautet, P.; Raybaud, P.; Euzen, P.; Toulhoat, H. Hydroxyl Groups on γ-Alumina Surfaces: A DFT Study. *J. Catal.* **2002**, *211* (1), 1–5. https://doi.org/10.1006/jcat.2002.3741.
(82) Monkhorst, H. J.; Pack, J. D. Special Points for Brillouin-Zone Integrations. *Phys. Rev. B* **1976**, *13* (12), 5188–5192. https://doi.org/10.1103/PhysRevB.13.5188.
(83) Blake, R. L.; Hessevick, R. E.; Zoltai, T.; Finger, L. W. Refinement of the Hematite Structure. *Am. Mineral.* **1966**, *51* (1–2), 123–129.
(84) He, Y.; Guo, F.; Yang, K. R.; Heinlein, J. A.; Bamonte, S. M.; Fee, J. J.; Hu, S.; Suib, S. L.; Haller, G. L.; Batista, V. S.; Pfefferle, L. D. In Situ Identification of Reaction Intermediates and Mechanistic Understandings of Methane Oxidation over Hematite: A Combined Experimental and Theoretical Study. *J. Am. Chem. Soc.* **2020**, jacs.0c07179. https://doi.org/10.1021/jacs.0c07179.
(85) Gouron, A.; Le Mapihan, K.; Camperos, S.; Al Farra, A.; Lair, V.; Ringuedé, A.; Cassir, M.; Diawara, B. New Insights in Self-Assembled Monolayer of Imidazolines on Iron Oxide Investigated by DFT. *Appl. Surf. Sci.* **2018**, *456*, 437–444. https://doi.org/10.1016/j.apsusc.2018.06.119.
(86) Essmann, U.; Perera, L.; Berkowitz, M. L.; Darden, T.; Lee, H.; Pedersen, L. G. A Smooth Particle Mesh Ewald Method. *J. Chem. Phys.* **1995**, *103* (19), 8577–8593. https://doi.org/10.1063/1.470117.
(87) Wang, J.; Wolf, R. M.; Caldwell, J. W.; Kollman, P. A.; Case, D. A. Development and Testing of a General Amber Force Field. *J. Comput. Chem.* **2004**, *25* (9), 1157–1174. https://doi.org/10.1002/jcc.20035.
(88) Gasteiger, J.; Marsili, M. Iterative Partial Equalization of Orbital Electronegativity—a Rapid Access to Atomic Charges. *Tetrahedron* **1980**, *36* (22), 3219–3228. https://doi.org/10.1016/0040-4020(80)80168-2.
(89) O'Boyle, N. M.; Banck, M.; James, C. A.; Morley, C.; Vandermeersch, T.; Hutchison, G. R. Open Babel: An Open Chemical Toolbox. *J. Cheminformatics* **2011**, *3* (1), 33. https://doi.org/10.1186/1758-2946-3-33.
(90) Jorgensen, W. L.; Chandrasekhar, J.; Madura, J. D.; Impey, R. W.; Klein, M. L. Comparison of Simple Potential Functions for Simulating Liquid Water. *J. Chem. Phys.* **1983**, *79* (2), 926–935. https://doi.org/10.1063/1.445869.
(91) Weiner, S. J.; Kollman, P. A.; Nguyen, D. T.; Case, D. A. An All Atom Force Field for Simulations of Proteins and Nucleic Acids: An All Atom Force Field. *J. Comput. Chem.* **1986**, *7* (2), 230–252. https://doi.org/10.1002/jcc.540070216.
(92) Case, D. A.; Cerutti, D. S.; Cheatham, T. E.; Darden, T. A.; Duke, R. E.; Giese, T. J.; Gohlke, H.; Goetz, A. W.; Greene, D.; Homeyer, N.; Izadi, S.; Kovalenko, A.; Lee, T. S.; LeGrand, S.; Li, P.; Lin, C.; J. Liu; Luo, R.; Mermelstein, D.; Merz, K. M.; Monard, G.; Nguyen, H.; Omelyan, I.; Onufrief, A.; Pan, F.; Qi, R.; Roe, D. R.; Roitberg, A.; Sagui, C.; Simmerling, C. L.; Botello-Smith, W. M.; Swails, J.; Walker, R. C.; Wang, J.; Wolf,

R. M.; Wu, X.; Xiao, L.; York, D. M.; Kollman, P. A. *AMBER 2017*; University of California, San Francisco, 2017.
(93) Halgren, T. A. The Representation of van Der Waals (VdW) Interactions in Molecular Mechanics Force Fields: Potential Form, Combination Rules, and VdW Parameters. *J. Am. Chem. Soc.* **1992**, *114* (20), 7827–7843. https://doi.org/10.1021/ja00046a032.
(94) Berg, A.; Peter, C.; Johnston, K. Evaluation and Optimization of Interface Force Fields for Water on Gold Surfaces. *J. Chem. Theory Comput.* **2017**, *13* (11), 5610–5623. https://doi.org/10.1021/acs.jctc.7b00612.
(95) Van Vleet, M. J.; Misquitta, A. J.; Stone, A. J.; Schmidt, J. R. Beyond Born–Mayer: Improved Models for Short-Range Repulsion in Ab Initio Force Fields. *J. Chem. Theory Comput.* **2016**, *12* (8), 3851–3870. https://doi.org/10.1021/acs.jctc.6b00209.
(96) Wang, X.; Ramírez-Hinestrosa, S.; Dobnikar, J.; Frenkel, D. The Lennard-Jones Potential: When (Not) to Use It. *Phys. Chem. Chem. Phys.* **2020**, *22* (19), 10624–10633. https://doi.org/10.1039/C9CP05445F.
(97) Martínez, L.; Andrade, R.; Birgin, E. G.; Martínez, J. M. PACKMOL: A Package for Building Initial Configurations for Molecular Dynamics Simulations. *J. Comput. Chem.* **2009**, *30* (13), 2157–2164. https://doi.org/10.1002/jcc.21224.
(98) Chen, Y.; Elhag, A. S.; Reddy, P. P.; Chen, H.; Cui, L.; Worthen, A. J.; Ma, K.; Quintanilla, H.; Noguera, J. A.; Hirasaki, G. J.; Nguyen, Q. P.; Biswal, S. L.; Johnston, K. P. Phase Behavior and Interfacial Properties of a Switchable Ethoxylated Amine Surfactant at High Temperature and Effects on CO_2-in-Water Foams. *J. Colloid Interface Sci.* **2016**, *470*, 80–91. https://doi.org/10.1016/j.jcis.2016.02.028.
(99) Chen, Y.; Elhag, A. S.; Poon, B. M.; Cui, L.; Ma, K.; Liao, S. Y.; Reddy, P. P.; Worthen, A. J.; Hirasaki, G. J.; Nguyen, Q. P.; Biswal, S. L.; Johnston, K. P. Switchable Nonionic to Cationic Ethoxylated Amine Surfactants for CO_2 Enhanced Oil Recovery in High-Temperature, High-Salinity Carbonate Reservoirs. *SPE J.* **2014**, *19* (02), 249–259. https://doi.org/10.2118/154222-PA.
(100) Dawczyk, J.; Russo, J.; Spikes, H. Ethoxylated Amine Friction Modifiers and ZDDP. *Tribol. Lett.* **2019**, *67* (4), 106. https://doi.org/10.1007/s11249-019-1221-4.

TOC Graphic